*Essential Readings in Light Metals: Aluminum Reduction Technology.*
Edited by Geoff Bearne, Marc Dupuis and Gary Tarcy.




# A WATER-MODEL STUDY OF THE LEDGE HEAT TRANSFER IN AN ALUMINIUM CELL

**John J.J. Chen, Chuck C. Wei & Antony D. Ackland***

Chemical & Materials Engineering Department
The University of Auckland
Private Bag 92019, Auckland, **NEW ZEALAND**

*Comalco Research Centre
P.O. Box 316, Thomastown, VIC 3074, **AUSTRALIA**

## Abstract

*A heat transfer probe was developed for studying the ledge heat transfer in a full-scale 3-D air-water model. Quantitative measurements were conducted to determine the bath/ledge heat transfer characteristics at various positions and different operating conditions. A similitude analysis was carried out to relate the measured point results to data available in the literature. A suggested range of heat transfer coefficients for the reduction cell is presented. Variation of the heat transfer were examined as a function of the anode bottom inclination, the position on the side ledge relative to the anode slot, and positions in the vertical direction.*

## Introduction

In Hall-Héroult cells for aluminium production, the sidewalls are usually maintained with a layer of frozen electrolyte which protects the lining material from the high temperature and highly corrosive cryolite-based electrolyte and the liquid aluminium. The sidewall ledge profile formed is dependent on the cell design, the materials of construction, and the overall hydrodynamic conditions in the molten bath, particularly in the sidewall region. However, the particular cell geometry, e.g. anode-ledge distance, anode angle, slot width, and operating parameters, e.g. current density and bath depth, will influence the cell fluid dynamics and affect the heat transfer hence resulting in the development of a steady-state ledge profile and thickness.

A properly designed cell will have a desirable heat distribution which causes a suitable steady-state ledge profile to form on the sidewalls so as to achieve the maximum possible service life. Apart from the protective and insulating characteristics, the freezing/remelting of the side ledge also serves a useful function in controlling the transient heat balance of the cell. Thus, although the "steady-state" ledge profile has been mentioned, the ledge profile and thickness undergo constant variations during the course of normal operation. Furthermore, a suitable shape of the side ledge also helps to maintain a stable metal pad and therefore allow stable cell operation and high-current efficiency.

The bath temperature and the dynamic variation of the side ledge are strongly influenced by the magnitude of the heat transfer coefficient between the bath and the side ledge. Literature available on studies of ledge heat transfer and the relevant particulars have been summarized[1]. It was found that a wide range of heat transfer coefficients was reported, ranging from 116 to 4000 W/m$^2$ K in the bath layer, and 20 to 1478 W/m$^2$ K for the ledge surface submerged in the metal layer. It is obvious that in most of these works, the heat transfer coefficients are not only scattered widely, but also provide insufficient insight into the mechanism of ledge heat transfer. Moreover, the effects of the relative position along the side ledge, and the changing configuration and operating parameters, on heat transfer coefficients are lacking. Thus, more refined predictions of the heat transfer coefficients are required for cell design and process control.

Due to the complex geometry and flow conditions in an aluminium cell, it is difficult to apply existing empirical equations available in standard textbooks to obtain reliable heat transfer coefficients. Furthermore, due to the high temperature, high corrosive and opaque environment of the operational cell, direct measurements are difficult to perform in industrial cells. There are also difficulties in determining these heat transfer coefficients in laboratory-scale cells where geometric similarity is not observed. Thus the flow patterns in these laboratory-scale cells will not represent the actual industrial situations. Appropriately designed heat transfer probes installed in a low-temperature model cell can be an effective and economic way of measuring the bath/ledge heat transfer.

A heat transfer probe had previously been explored and its accuracy was verified under standard conditions of natural convection and forced convection[2]. Prior to carrying out tests in the full scale 3-D model, preliminary tests on the bath/ledge heat transfer were conducted in a 2-D model cell at various positions and operating parameters. The results from the 2-D model cell have further confirmed the reliability of the heat transfer probe and its measurement techniques were established[2]. In the 2-D model, the results obtained are under rather constrained conditions. For example, only the condition of gases being released into the side channel can be studied. The variation of bath depth is also limited. The effect of the unequal current density at adjacent anodes cannot be simulated.

As a 2-D model is, in effect, a representation of a vertical "slice" of the sidewall, effects due to the relative positions with respect to the anode-anode slot and the effects of slot gap cannot be studied. Thus, a more detailed study of ledge heat transfer using a 3-D model cell was necessary.

### Similarity Analysis

The bath/ledge heat transfer coefficients for an industrial cell had been evaluated from correlations for turbulent flows over flat plates[3,4]. The relationship for the local Nusselt number may be expressed by Eqn.(1)[5] which was obtained from the Colburn analogy.

$$Nu_x = 0.0292\ Re_x^{0.8}\ Pr^{1/3} \qquad (1)$$

While this equation had been used in the calculation of bath/ledge heat transfer, its predicted values have not been substantiated. Nevertheless, it is believed that the functional forms of this equation are still valid and therefore will be used in the following analysis. It is noted that the above correlation is applicable only if the heat transfer takes place over the entire plate. If the leading section of the plate is unheated for a distance of $x_o$ from the leading edge as illustrated in Figure 1, a correction must be made. An analytical expression has been developed as shown in Eqn.(2) for the local Nusselt number on a flat plate with such a stepwise discontinuity in the surface-temperature[5]. Scesa and Sauer[6] have studied heat transfer from plates with a step increase in temperature on the plate surface. Using the leading length correction, they found that the experimental results were correlated with the Colburn equation, as shown in Eqn.(2), within ±6 percent.

$$Nu_x = 0.0292\ Re_x^{0.8}\ Pr^{1/3}\left[1 - \left(\frac{x_o}{x}\right)^{39/40}\right]^{-7/39} \qquad (2)$$

At $x=x_o$, there is a stepwise change in temperature. The last term of Eqn.(2) denotes the correction to account for the unheated leading section of the plate. This consideration is somewhat similar to our 3-D model using a heat transfer probe because the heated probe provides a step increase in the temperature on the plate surface as illustrated in Figure 2. The actual situation is more complex as the bath flow is a circulating one rather than being parallel to the ledge. Thus, in reality, the boundary layer development will differ from that as shown in Figure 2.

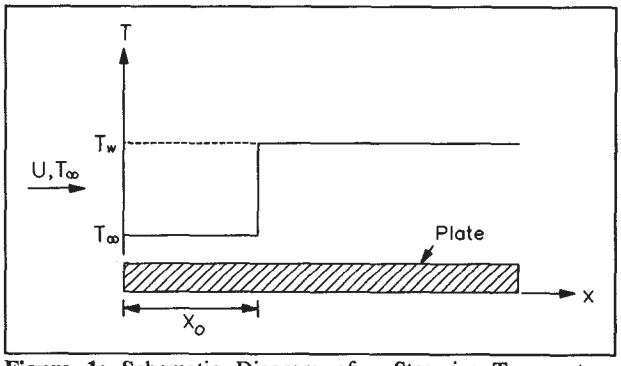


**Figure 1:** Schematic Diagram of a Stepwise Temperature Change at a Point $x_o$ from the Leading Edge of a Flat Plate.

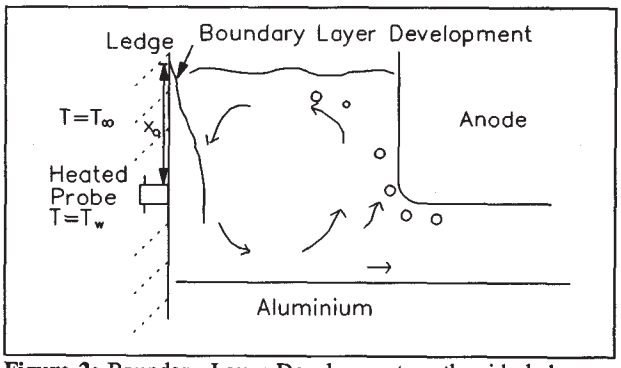


**Figure 2:** Boundary Layer Development on the side ledge.

Eqn. (3) may be written for the bath heat transfer along the ledge surface based on Eqn.(1), while Eqn.(2) may be written for the water model as Eqn.(4) in which a leading section when a distance $x_o$ of the plate is unheated.

$$\frac{h_{b,x}\,x_b}{k_b} = 0.0292\left[\frac{u_b\,x_b}{\nu_b}\right]^{0.8} Pr_b^{1/3} \qquad (3)$$

$$\frac{h_{w,x}\,x_w}{k_w} = 0.0292\left[\frac{u_w\,x_w}{\nu_w}\right]^{0.8} Pr_w^{1/3}\left[1 - \left[\frac{x_o}{x_w}\right]^{39/40}\right]^{-7/39} \qquad (4)$$

where $\nu$ is the kinematic viscosity. Dividing Eqn.(3) by Eqn.(4),

$$\frac{h_{b,x}}{h_{w,x}} = \left[\frac{k_b}{k_w}\right]\left[\frac{u_b\,\nu_w}{u_w\,\nu_b}\right]^{0.8}\left[\frac{Pr_b}{Pr_w}\right]^{1/3}\left[\frac{x_w}{x_b}\right]^{0.2}\left[1-\left[\frac{x_o}{x_w}\right]^{39/40}\right]^{7/39} \qquad (5)$$

With geometric similarity, using a full-scale model, the corresponding geometric dimensions of the 3-D model and the operating cell are the same, ie., $x_w = x_b$. Furthermore, if $u_b = u_w$, it can be assumed that kinematic similarity exists and Eqn.(5) becomes,

$$h_{b,x} = h_{w,x}\left[\frac{k_b}{k_w}\right]\left[\frac{\nu_w}{\nu_b}\right]^{0.8}\left[\frac{Pr_b}{Pr_w}\right]^{1/3}\left[1-\left[\frac{x_o}{x_w}\right]^{39/40}\right]^{7/39} \qquad (6)$$

However, if the velocity is influenced by the fluid properties, the correlation of Dernedde and Cambridge[3] which was derived for a 2-D model, may be used to examine the results. The average circulation velocity, $u_c$, as a function of the cell geometry and fluid properties can be calculated from

$$u_c = 0.173\ (g * GF)^{0.458}\ AI^{0.467}\ ALD^{-0.258}\ \nu^{-0.044} \left[ \frac{\sigma}{\rho} \right]^{-0.165} \quad (7)$$

where GF is the gas flow rate per unit length of the anode edge and all variables are expressed in c.g.s. unit. The velocity at the side ledge was related to the average circulation velocity by

$$u = u_c \left[ \frac{2(AI)}{ALD} \right]^{0.25} \quad (8)$$

Combining Eqns.(7) and (8), the velocity at the side ledge can be expressed in SI units as follows.

$$u = 0.585\ GF^{0.458}\ AI^{0.717}\ ALD^{-0.508}\ \nu^{-0.044} \left[ \frac{\sigma}{\rho} \right]^{-0.165} \quad (9)$$

When the vertical(gas-induced) bath circulation is superimposed on a horizontal(magnetically induced) flow, the resultant velocity vector near the side ledge is given by a vector addition of the vertical and the horizontal components, as shown in the following equation.

$$u = u_v \left[ 1 + \left( \frac{u_h}{u_v} \right)^2 \right]^{1/2} \quad (10)$$

For purely gas-induced flow, $u_h = 0$, and hence u is equal to $u_v$. Substitution of Eqn.(9) into Eqn.(5) and re-arranging gives

$$h_{b,x} = h_{w,x} \left( \frac{k_b}{k_w} \right) \left( \frac{\nu_b}{\nu_w} \right)^{-0.8352} \left( \frac{\frac{\sigma_b}{\rho_b}}{\frac{\sigma_w}{\rho_w}} \right)^{-0.132} \left( \frac{Pr_b}{Pr_w} \right)^{1/3} \left[ 1 - \left( \frac{x_o}{x_w} \right)^{39/40} \right]^{7/39} \quad (11)$$

A comparison of the relevant properties for water and industrial bath is shown in Table 1. A correction must therefore be made for the different thermal and physical properties, using Eqn.(6) or Eqn.(11).

The fluid flow boundary layer experienced by the heat transfer probe is much thicker than is normally expected because the flow had begun much further upstream. Furthermore, the development of this boundary layer is rather complex because the flow is recirculating, induced by the rising gas bubbles at the anode edge[2]. Thus, one can expect the fluid boundary layer to be thicker than that expected for a uni-directional flow over a distance equal to the bath level.

The heat transfer probes, A, B, and C, mounted on the perspex side ledge, were positioned at levels of 180, 120 and 60mm above the *solid* metal/bath interface which will be referred to hereinafter as the *high*, *middle*, and *low* positions along the side ledge, respectively. The locations of the heat transfer probes are defined as shown in Figure 3. For example, $H_A$ , $M_A$ and $L_A$ represent the heat transfer probe A, opposite the Anode 1, located at the *high*, *middle*, and *low* positions, respectively.

To obtain the heat transfer coefficient in the industrial bath at the same operating parameters, the results for $h_{b,x}$ obtained from the water model experiment need to be converted by a factor of 0.49, 0.42 and 0.38 corresponding to the *high*, *middle* and *low* positions respectively, if $u_b = u_w$ according to Eqn.(6). However, if the velocity is influenced by the fluid properties, a factor of 0.50, 0.43 and 0.39 must be applied, according to Eqn.(3.11). It is noted that the correction factors in these two cases are essentially the same.

Table 1 Physical Properties of Water and Industrial Bath

| Property | Industrial Bath | Water |
|---|---|---|
| Bath temp (°C) | 970 | 20 |
| Density (kg/m$^3$) | 2050 | 1000 |
| Kinematic viscosity (m$^2$/s) | $1.22*10^{-6}$ | $1.0*10^{-6}$ |
| Thermal conductivity (W/m K) | 0.4 | 0.6 |
| Kinematic surface tension (m$^3$/s$^2$) | $6.3*10^{-5}$ | $7.3*10^{-5}$ |
| Prandtl number | 14.3 | 7.02 |

### Experiment Equipment

A 3-D physical model was set up with two full-scale anodes. The anode bottom consists of a polyethylene diffuser plate through which air is passed so as to simulate carbon dioxide gas evolution during electrolysis. 14 compartments with individual air supplies are provided so as to ensure uniform distribution of gas flow over the anode face. Water at room temperature simulates the liquid bath. A perspex plate was shaped so as to simulate a typical side ledge profile.

The anodes may be so arranged that the dynamic characteristics and flow field in the various regions of the cell such as the side channel, the slot area, the centre channel and the anode ledge gap, may be represented. In operating cells, the bath/ledge interface heat transfer has been observed as a quasi-steady state problem because the movement of the ledge due to freezing/remelting is normally about 0.1mm/min[7]. Hence, the perspex side ledge without the freezing/remelting process can represent reasonably well a typical operating ledge profile.

The metal phase was ignored with the assumption that the metal pad interface consists of a solid horizontal surface. Solheim *et al.*[8] indicated that it can be assumed that the absence of the metal phase did not affect the fluid dynamics at or near the anode. Their computational results also showed that the difference in the magnetically induced metal motion had no significant effect on bath circulation. Bilek *et al.*[9] qualitatively assessed the influence due to MHD and gas driven forces by using a 3-D computational model. The results showed that the majority of the fluid flow at the sidewalls was due to gas induced forces. Using a 2-D ice-water-hydrocarbon model, the water-tetrachloroethylene interfacial wave was generated by a piston wave-maker placed on the side opposite to the ice in the modelling cell. Chen *et al*[10] also found that the heat transfer coefficients were very high in the vicinity of the liquid-liquid interface. However, the ice-ledge away from the interfacial region was not significantly influenced.

Figure 3 shows a schematic diagram of the 3-D water model with the typical geometries found in an operating cell. Three heat transfer probes situated at various fixed positions on the side ledge. Thermocouple readings from the heat transfer probes were obtained using data acquisition system. The heat transfer coefficients measurement were obtained under steady-state conditions.

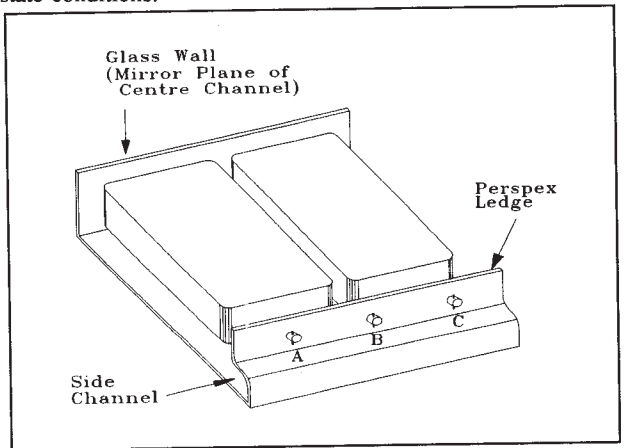


**Figure 3:** Schematic Diagram of the 3-D Model with Locations of the Heat Transfer Probes as Indicated by "A", "B" and "C".

The two anodes in the 3-D model were positioned at a distance of 100mm from the glass wall, ie. representing half the centre-channel width, and the anode-anode slot width was 50mm. Three heat transfer probes were mounted on the perspex ledge as illustrated in Figure 3. In addition, each probe may be placed at one of the 3 positions along a vertical plane perpendicular to the ledge, as indicated in Figure 4.

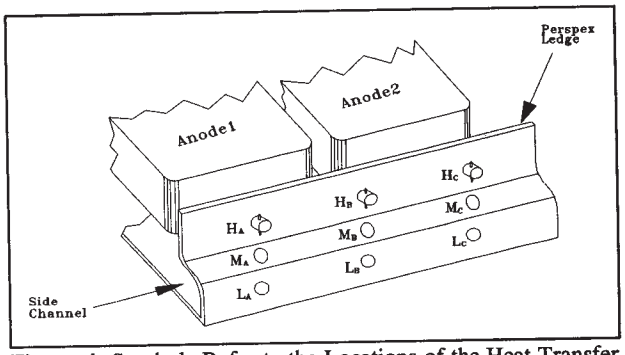


**Figure 4:** Symbols Refer to the Locations of the Heat Transfer Probes.

### Results and Discussion

The model cell was set up with the anodes and the calibrated heat transfer probes as arranged in Figure 5. The scope of this work is to obtain quantitative information on the magnitude of the bath/ledge heat transfer, and a qualitative appreciation of the influence of the various operating parameters. For each location of the probes, the effects of anode-ledge distance, current density and bath depth, on heat transfer were studied. The variation of anode arrangements such as slot width and anode angle will also be discussed.

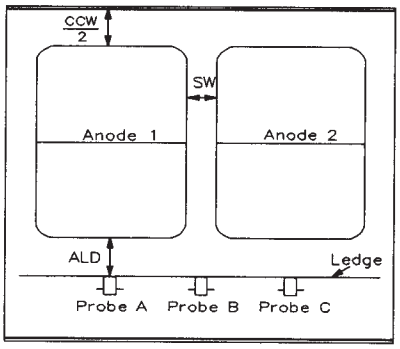


**Figure 5:** Plan View of 3-D Model Cell Showing the Relative Locations of the Heat Transfer Probes.

The geometry in the *standard* configuration is as follows:

| | |
|---|---|
| Anode-cathode Distance(ACD): | 50mm |
| Centre-channel width(CCW): | 200mm |
| Slot Width(SW): | 50mm |
| Anode-ledge Distance(ALD): | 150mm |
| Bath Depth(BD): | 200mm |
| Probe Position: | 60,120,180mm |
| Anode Angle: | 0° |

It is important to note that the heat transfer coefficients presented in the following have not been corrected by the conversion factors derived through the similarity analysis for the actual cell as given above.

### 1. *Effect of Anode-ledge Distance*

Anode-ledge distances investigated were 50, 100, 150, 200, 250 and 300mm for the three vertical positions of *high*, *middle* and *low* for each of the heat transfer probes and the results are shown in Figures 6 to 8. The anode-cathode distance(ACD) and slot width were kept constant at 50mm.

Generally it is observed that with a decrease in the anode-ledge distance(ALD), there is an increase in the heat transfer coefficients measured at the three vertical positions of the probe. This is because as the ALD is decreased, there is a smaller volume of electrolyte(water) available in the anode-ledge space to dissipate the energy caused by the anode gas evacuation. Bearne *et al*[11] confirmed in their 3-D model cell that bath velocities towards and down the sidewall adjacent to the anode slot were 34% and 23% higher respectively for the narrow cell with a reduction of the anode to sidewall distance from 450 to 250mm. It is reasonable to deduce that this will increase the bath/ledge heat transfer coefficients in the bath zone.

It is observed that a highly turbulent region exists in the anode slot. Gas-driven flow fluctuations are also found coming out of the slot, near the bath surface. The free surface undergoes significant pulsation, increasing the rate of "surface renewal", and therefore a significant reduction in the thermal boundary layer. This results in a remarkably high heat transfer coefficient at the *high* positions.

There is no such highly turbulent flow at positions below the *high* position. The heat transfer coefficients at the *middle* and the *low* positions are lower than at the *high* position. Furthermore, at lower locations, the gas-driven flow out of the slot does not cause large scale eddies as at the *high* position. Thus, the heat transfer coefficients measured adjacent to the slot have a more significant decrease than those measured opposite the anodes.

It must be emphasized that in actual plant operations, it would not be possible to have anodes with uniform gas evolution along the entire periphery of the anode. In the model cell, it was found that fewer bubbles are released from Anode 1 than from Anode 2[2]. This will cause a force imbalance around the region of the anode-ledge gap. The gas evacuation from Anode 2 causes higher turbulence, from gas-driven flow past probe C, located opposite Anode 2. The heat transfer coefficients, measured by probe C, are higher than those measured by probe A, located opposite Anode 1. On the basis of the configuration of these anode settings, the heat transfer coefficients at different positions reflect the magnitude of the turbulence in the anode-ledge gap region.

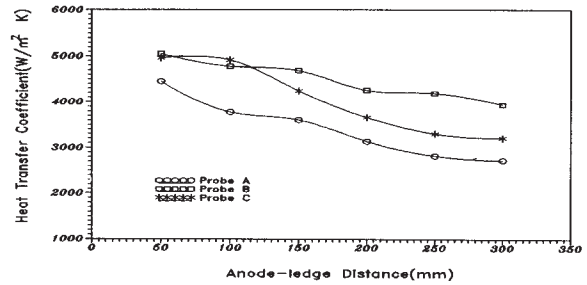


**Figure 6:** 3-D Heat Transfer Measured at an ALD=50-300mm, at *High* Position of the Side Ledge.

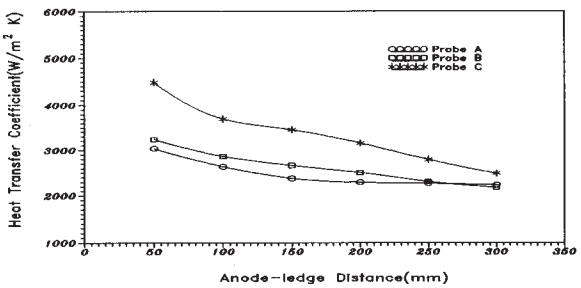


**Figure 7:** 3-D Heat Transfer Measured at an ALD=50-300mm, at *Middle* Position of the Side Ledge.

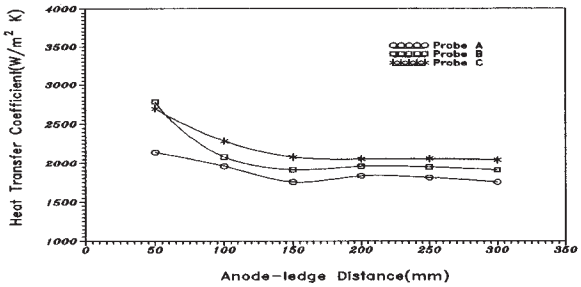


**Figure 8:** 3-D Heat Transfer Measured at an ALD=50-300mm, at *Low* Position of the Side Ledge.

### 2. *Effect of Current Density*

In aluminium electrolysis, anodes are continuously consumed by electrochemical reactions mainly on the bottom face, while some air oxidation also occur on the sides. Consequently, spent anodes (butts) have to be replaced with new ones on a regular basis. A new anode will be cold and causes electrolyte to freeze onto the immersed surface of the anode. While this frozen layer remains, the anode will not carry any significant amount of current. As the frozen electrolyte gradually remelts, current will begin to flow through the anode until a steady-state value is reached.

Measurements and modelling have shown that after introducing a new anode, the freeze will extend down to the metal pad within 90-100 minutes but it will take more than 24 hours for the freeze to totally remelt[12]. Thus, for a certain period of time, anodes adjacent to a newly-set one will carry a proportionately higher current following anode replacement. Thus, the effects of different current densities for both anodes, varied from 0.4 to 1.0 A/cm$^2$, were studied.

Figures 9 to 11 show the effects of current densities on the bath/ledge heat transfer at different positions at an anode-ledge distance of 100mm. As expected, the momentum transfer from the bubble release to the bath has been increased as the current density is increased from 0.4 to 1.0 A/cm$^2$ which results in an increase in the heat transfer coefficient. The heat transfer coefficients measured opposite Anode 2(probe C) are greater than those measured at other locations, probe A and B.

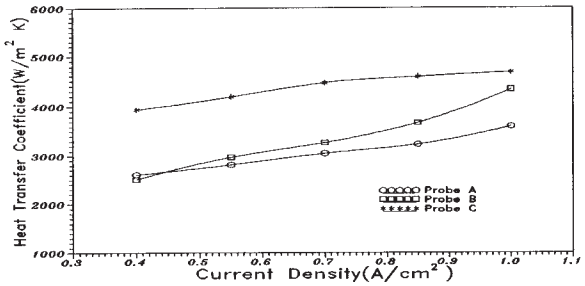


**Figure 9:** 3-D Heat Transfer Measured at an CD=0.4-1.0, at *High* Position of the ALD=100mm.

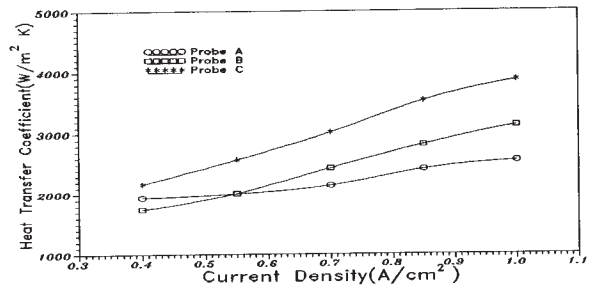


**Figure 10:** 3-D Heat Transfer Measured at an CD=0.4-1.0, at *Middle* Position of the ALD=100mm.

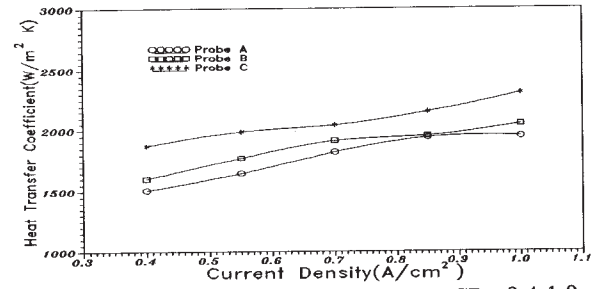


**Figure 11:** 3-D Heat Transfer Measured at an CD=0.4-1.0, at *Low* Position of the ALD=100mm.

### 3. *Effect of Bath Depth*

In the following tests, where the effects of bath depths were examined, a constant CD of 1.0 A/cm$^2$ was used. Figure 12 shows the effects of increasing bath depth from 200 to 300mm at an ALD of 100 measured at the *high* position. No readings were taken for the bath depths of 150 and 100mm as the probes at the *high* position were not immersed in water at these bath depths. For probe positions $H_A$ and $H_C$ which are directly opposite the centre of the anode, it can be seen that increasing the bath depth results in a decrease in the heat transfer coefficient. This is because the turbulent circulating flow pattern near the bath surface occurs above the probe location as the bath depth is increased. However, the heat transfer coefficients measured opposite the slot increase with increasing bath depth and have the highest heat transfer coefficient at a bath depth of 300mm. As has already been noted, the heat transfer coefficients measured adjacent to the slot are higher than those measured opposite the anodes. This is because the bubble shape may be better established in the anode slot region of the higher bath depth which results in increased eddying flows adjacent to the slot.

Figure 13 illustrates the heat transfer coefficients measured at the *middle* position, 120mm above the *solid* metal/bath interface, as the bath depth is increased from 150 to 250mm. The bath/ledge heat transfer coefficients opposite the slot increased with bath depth and have the highest values at a bath depth of 250mm, while at the same time, the heat transfer coefficients measured opposite both the anodes decreased. It is noted that while increasing the bath depth from 200 to 250mm, the probes adjacent to both anodes show no significant variation in heat transfer coefficients compared with the region of 150 to 200mm.

As the bath depth increases from 100 to 200mm, the same trends also occur when the location of the probe on the side ledge is moved down to the *low* position, 60mm above the *solid* metal/bath interface, as shown in Figure 14. The bath/ledge heat transfer coefficient measured opposite the slot shows an insignificant variation initially and then increases until it reaches a maximum heat transfer coefficient at a bath depth of 200mm.

Comparison of the heat transfer coefficient at any ledge position but with different bath heights shows that an increase in bath height causes a decrease in the turbulence opposite the anodes and hence a decrease in the bath/ledge heat transfer at probes A and C. This is due to the larger volume of electrolyte(water) available at high bath depths to dissipate the energy so that the effect of turbulence is reduced. Furthermore, the highly turbulent circulating flow which occurs near the free surface had risen to a higher level and thus has its effects experienced at a higher level on the ledge. However, the increased anode immersion as the bath depth is increased results in intense turbulence appearing in the slot area as well as an increase in the bath velocity directed out of the slot area resulting in an increase in the bath/ledge heat transfer as measured at probe B.

Previous studies using 2-D models[1,2] indicated that as the bath depth was increased, the turbulence caused by the bubbles released from the anode increased and resulted in higher heat transfer. It is, therefore, clearly shown that the gas released into the side ledge in a 2-D sliced anode model merely reflects part of the flow pattern in a 3-D full scale model.

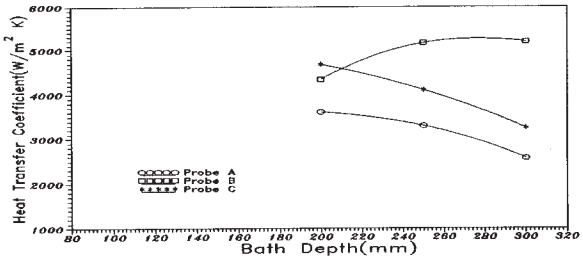


**Figure 12:** 3-D Heat Transfer Measured at an BD=200-300mm, at *High* Position of the ALD=100mm.

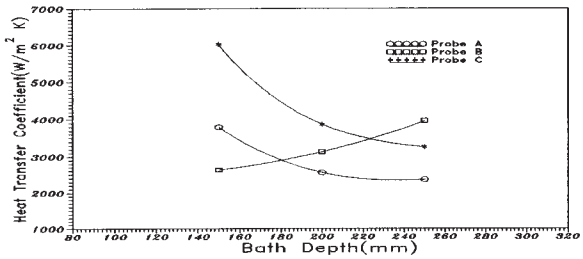


**Figure 13:** 3-D Heat Transfer Measured at an BD=150-250mm, at *Middle* Position of the ALD=100mm.

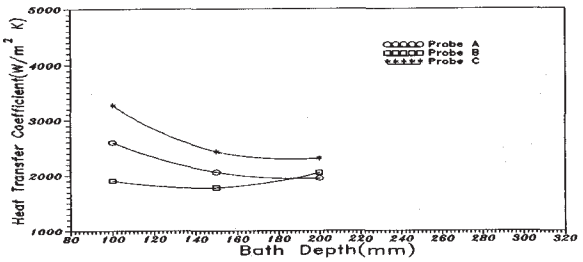


**Figure 14:** 3-D Heat Transfer Measured at an BD=100-200mm, at *Low* Position of the ALD=100mm.

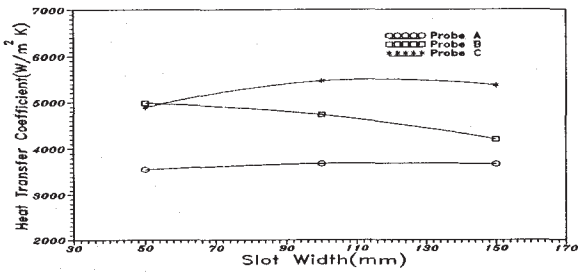


**Figure 15:** 3-D Heat Transfer Measured at the *High* Position of the Side Ledge with the Variation of Slot Width at 50-150mm. Anode-ledge Distance is 100mm.

### 4. *The Effect of Anode Slot*

During aluminium electrolysis, several possible reactions occur on the anode surface consuming the anode block. Such reactions include electrochemical, Boudouard and airburn reactions. 75% of the anode block is consumed through the primary electrochemical reaction[13]. The effective anode area for electrolysis will be reduced if any of these reactions occur on the vertical faces of anode. Carbon consumption measurements show that the reduction to the anode bottom face dimensions is of the order of 12% over the anode life[14].

As the anode bottom surface area is reduced, the slot widths between anodes increase affecting the gas evolution and hence the flow pattern in the anode-ledge region. By changing the slot width, it was observed that the heat transfer coefficient varied along the side ledge[15]. Bilek *et al*[9], in their numerical model, also indicated that increasing the slot width has the effect of reducing the local heat transfer on the sidewall near the slots. However, there are no quantitative results reported in the literature. Thus, it is necessary to study the effect of slot width, which is related to the anode age, on the ledge heat transfer.

The effects of slot width at the *high* position on heat transfer along the side ledge are illustrated in Figure 15. These results confirm what was observed in the numerical model[9] and quantify the variation in ledge heat transfer with respect to position. It is obvious that with increasing slot width, the probe B located adjacent to the slot shows a pronounced decrease in the heat transfer at various positions of the side ledge.

Irrespective of the slot width, the higher position of the side ledge gives a higher heat transfer coefficient. This indicates that the highly turbulent flow near the bath surface has a strong influence on the heat transfer at higher positions. However, the probes positioned opposite the anodes generally show insignificant variation in the heat transfer coefficient. The heat transfer coefficient measured at probe C is higher than that measured at probe A. This is due to the difference of gas evolution on the two anodes which are installed in the existing model. Further discussions on the lower positions and anode-ledge distance of 200mm were given elsewhere[10].

### 5. *Influence of Anode Slope*

During cell operation, since the metal pad develops a contour due to the magnetic effect present, the anode is consumed and shaped so as to match the metal pad profile. Hence, an inclined surface on the anode bottom is formed with service. Newly installed anodes will have a bottom surface close to or at the horizontal level, while anodes after a certain period of service will have a bottom surface inclined by a few degrees.

To simulate the effects of anode age, the anode inclination was varied from the horizontal to some slight angle with respect to either the side ledge or the centre-channel region. This anode inclination affects the behaviour of bubble formation and also causes a greater buoyancy force to act in the direction of the inclination resulting in a change in the intensity of turbulent circulation in the anode-ledge region.

The effects of anode slope on the ledge heat transfer at the *high* position are illustrated in Figure 16. For an anode inclined from -2 to 2 degrees, it is clear that at the *high* position the heat transfer coefficient measured adjacent to the anode slot (probe B) is higher than those measured opposite the anodes (probes A and C) irrespective of the anode slope. Decreasing the anode slope towards the centre-channel, e.g. from 2° to 1°, or increasing the anode inclination with respect to the side ledge, generally has the effect of causing a larger portion of the bubbles to be released to the anode-ledge region. Thus, a higher turbulent eddy is generated which causes higher ledge heat transfer.

For an anode which is slightly inclined from the horizontal to -0.5 degree(i.e. inclined upwards at the side ledge), there is a significant increase in the ledge heat transfer on the ledge directly facing the slot(probe B). However, the increase in heat transfer at positions opposite the anodes is much lower. It is of interest to note that for an anode inclined at greater than -0.5 degree, the heat transfer coefficient measured at probe B facing the slot is reduced. The increase in heat transfer at a low anode inclination of around -0.5 degree is possibly caused by a significant increase in the gas flow into the slot region as the anode inclination changed from the horizontal to -0.5 degree. Further increase in anode inclination caused the gas to flow almost uni-directionally toward the side ledge, with a less eddying flow existed in the anode slot region. This possibly explains why the heat transfer is reduced in the regions opposite the slot at such higher inclinations. Further discussion on the lower positions and the anode-ledge distance of 200mm were presented elsewhere[10].

Referring to the results obtained from the 2-D model[2], it was shown that similar trends were observed in the effect of the anode inclination on the bath/ledge heat transfer with respect to the positions and anode-ledge distance. However, a substantial variation in ledge heat transfer is obtained in the 3-D model cell. Apart from the anode inclination towards the centre channel, more detailed measurements on the side ledge adjacent to the anode slot are only possible using the 3-D model. Thus, a 2-D model which represents at best a transverse section of half an anode and a vertical *slice* of the side ledge is inadequate. A 3-D model will reflect more closely the flow pattern in actual cells to provide more reliable quantitative results.

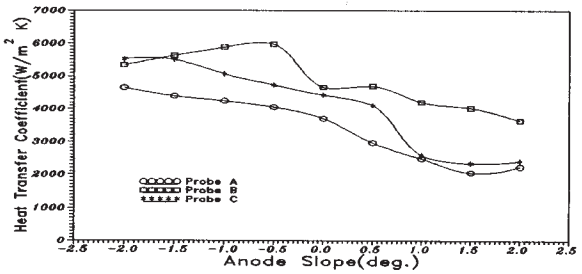


**Figure 16:** 3-D Heat Transfer Measured at the *High* Position of the Side Ledge with the Variation of Anode Slope at -2 to 2 Degree. Anode-ledge Distance is 100mm. Negative Degree Represents Anode Tilt towards the Side Ledge.

### *6. Summary of Heat Transfer Dependence*

The range of heat transfer coefficients measured at typical operating parameters of CD=1.0 A/cm$^2$, BD=200mm, ALD=100~200mm, SW=50mm and horizontal anodes are summarised in Table 2.

Table 2 3-D Heat Transfer Coefficient Ranges at Typical Operating Parameters

| Position | Probe A | Probe B | Probe C |
|---|---|---|---|
| *High* | 3132~3776 | 4249~4778 | 3658~4915 |
| *Middle* | 2011~2636 | 2467~3132 | 2939~3861 |
| *Low* | 1752~1959 | 1909~2080 | 2051~2305 |

Based on a similarity analysis, the heat transfer coefficients obtained from a 3-D water model needs to be multiplied by a factor of 0.5, 0.43 and 0.39 respectively for the *high*, *middle* and *low* positions in order to relate to the results for an operating cell. The corrected results are given in Table 3. The heat transfer coefficients vary over a wide range and depend on the positions of the side ledge and the operating parameters.

Table 3 Estimated Bath/ledge Heat Transfer Coefficients for the Reduction Cell

| Bath/ledge Position | Location A# | Location B | Location C |
|---|---|---|---|
| *High* | 1566~1888 | 2125~2389 | 1829~2458 |
| *Middle* | 865~1133 | 1061~1347 | 1264~1660 |
| *Low* | 683~764 | 745~811 | 800~899 |

# Locations A and C represent the positions adjacent to the anodes while probe B denotes the position opposite the slot.

## Conclusions

Quantitative measurements of the bath/ledge heat transfer were carried out using calibrated heat transfer probes installed in a full-scale 3-D water model. The measured heat transfer coefficients depend on the ledge positions and operating parameters such as the anode-ledge distance, current density, bath depth, and anode life associated with anode slot and anode inclination. It is shown that the configuration of the anode setting and anode life affects the heat transfer on the adjacent bath/ledge interface. The results show that at the higher positions on the side ledge, the heat transfer is higher, and there is a variation in heat transfer in the vertical and in the lateral position. Hence, it is expected that the ledge profile will take on a shape in compliance with the heat transfer variation.

In order to obtain actual operating data in a reduction cell, a similarity analysis had been performed. Using the correction factors derived from this analysis, meaningful results for the bath/ledge heat transfer can be obtained. The suggested range of heat transfer coefficients for the reduction cell shows position-dependence along the side ledge as well as variations with operating parameters.

## Acknowledgements

Financial support by Comalco Research & Technology and the University of Auckland Research Committee is gratefully acknowledged.

## References

1. Chen J.J.J., Wei C.C., Thomson S., Welch B.J. and Taylor M.P., "A Study of Cell Ledge Heat Transfer Using an Analogue Ice-water Model", ***AIME Light Metals***, pp.285-293, 1994.
2. Wei C.C., "Modelling of Ledge Heat Transfer in Hall-Héroult Cells", Ph.D Thesis in Preparation, The University of Auckland.
3. E. Dernedde and E. L. Cambridge, "Gas Induced Circulation in an Aluminium Reduction Cell", ***Light Metals***, pp.111-122, 1975.
4. J. Li and Z. Qiu, "Computer Simulation of the Shape of Ledge in Aluminium Electrolysis Cell", ***J. of Northeast University of Technology***, vol.**10**, pp.232-237, 1989.(in Chinese).
5. J. G. Knudsen and D. L. Katz, "Fluid Dynamic and Heat Transfer", Robert E. Krieger Publishing Co., New York, 1979.
6. S. Scesa and F. M. Sauer, "An Experimental Investigation of Convective Heat Transfer to Air From a Flat Plate with a Stepwise Discontinuous Surface Temperature", ***Trans. ASME***, vol **74**, pp.1251-1255, 1952.
7. M. P. Taylor and B. J. Welch, "Bath/Freeze Heat Transfer Coefficients: Experimental Determination and Industrial Application", ***Light Metals***, pp.781-789, 1985.
8. A. Solheim, S. T. Johansen, S. Rolseth and J. Thonstad, "Gas Induced Bath Circulation in Aluminium Reduction Cells", ***J. Appl. Electro.***, vol.**19**, pp.703-712, 1989.
9. M. M. Bilek, W. D. Zhang and F. J. Stevens, "Modelling of Electrolyte Flow and its Related Transport Processes in Aluminium Reduction Cells", ***Light Metals***, pp.323-330, 1994.
10. Chen J.J.J., Wei C.C. and A. D. Ackland, "Use of Models in the Study of Ledge Heat Transfer", ***5th Australasian Aluminium Smelting Technology Workshop***, Oct. 1995.
11. G. Bearne and A. Jenkin, L. Knapp and I Saeed, "The Impact of Cell Geometry on Cell Performance", ***Light Metals***, pp.375-380, 1995.
12. K. Grjotheim, B. J. Welch and M. P. Taylor, "Relating Operating Strategy and Performance in Aluminium Smelting Cells - An Overview", ***Light Metals***, pp.255-260, 1989.
13. A. M. Fitchett, B. J. Welch, J. T. Keniry and B. A. Sadler, "Reducing Anode Carbon Consumption in Smelting Cells", ***Aust. Bicentennial Int. Conf. Process Industries - CHEMECA '88***, pp.274-279, 1988.
14. G. C. Barber, Ph.D. Thesis, The University of Auckland, New Zealand, 1992.
15. P. Utne, "Freeze Profile in Side-break Cells - Calculations and Measurements", ***Light Metals***, pp.359-371, 1982.